Biosensors and Bioelectronics 144 (2019) 111664

Contents lists available at ScienceDirect

Biosensors and Bioelectronics

journal homepage: www.elsevier.com/locate/bios

Signal-on electrogenerated chemiluminescence biosensor for ultrasensitive detection of microRNA-21 based on isothermal strand-displacement polymerase reaction and bridge DNA-gold nanoparticles

Aiping Cui, Jianwei Zhang, Wanqiao Bai, Huiping Sun, Lin Bao, Fen Ma, Yan Li*

Key Laboratory of Synthetic and Natural Functional Molecule Chemistry of Ministry of Education, College of Chemistry and Materials Science, Northwest University, Xi'an, Shaanxi, 710127, China

ARTICLE INFO

Keywords:
Electrogenerated chemiluminescence
miRNA-21
Isothermal strand-displacement polymerase reaction
Bridge DNA-AuNPs nanocomposites

ABSTRACT

MicroRNA-21 (miRNA-21) is a promising diagnostic biomarker for breast cancer screening and disease progression. A sensitive and selective strategy for the quantitative determination of miRNA-21 is of great significance in the early diagnosis of cancers. Herein, a novel electrogenerated chemiluminescence (ECL) biosensor was designed for the detection of miRNA-21 with dual signal amplification based on isothermal strand-displacement polymerase reaction (ISDPR) and bridge DNA-gold nanoparticles (AuNPs) nanocomposites. The ECL biosensor was fabricated by self-assembling a thiolated capture probe (SH-CP) on the surface of a gold electrode. The target miRNA-21 initiated the phi29 DNA polymerase-mediated ISDPR, which could generate large numbers of single-stranded DNA (assistant DNA) with accurate and comprehensive nucleotide sequences. The assistant DNA was captured by the SH-CP self-assembled on the Au electrode and further hybridized with bridge DNA-AuNPs nanocomposites, more biotins can be captured on the electrode surface. Afterward, a streptavidin-modified Ru $(bpy)_3^{2+}$ complex (SA-Ru) was bound to the bridge DNA-AuNPs nanocomposites via a specific interaction between biotin and streptavidin to produce a strong ECL signal. The ECL intensity was logarithmically proportion to the concentration of target miRNA-21 over a range from 0.01 fM to 10,000 fM with a detection limit of 3.2 aM. The proposed ECL biosensor was successfully applied to detect miRNA-21 in total RNA samples extracted from human breast cancer cells, and it showed great potential for early cancer diagnosis based on miRNA as a biomarker.

1. Introduction

MicroRNAs (miRNAs) are endogenous and noncoding single-stranded RNAs with lengths of 18–25 nucleotides (nt) (Git et al., 2010) that play considerable roles in biological processes such as cell regulation, tumor metastasis, stem-cell differentiation renewal, and viral replication (Li et al., 2017). MiRNAs have been evaluated as significant biomarkers for cancer diagnosis or prognosis (Deng et al., 2017). In early studies, some traditional techniques, including Northern blotting (Lee and Ambros, 2001), microarrays (Liang et al., 2005; Yuen et al., 2002), and real-time polymerase chain reaction (RT-PCR) (Chen et al., 2005) have been reported for miRNA detection. However, these techniques present the disadvantages of time-consuming, labor-intensive, and expensive, which limits their application in early diagnosis (Hansen et al., 2013). In addition, the content of miRNA in peripheral blood plasma and serum often range from the femto-to nanomolar levels (Yang et al., 2018a; Tian et al., 2018). Therefore, the development of a highly sensitive method and signal enhancement strategy for miRNA detection is greatly required.

Electrogenerated chemiluminescence (ECL) biosensing method, owing the merits of high sensitivity, wide detection range and easy operation (Liu et al., 2014b, 2015), has attracted significant interest and offers new opportunities for applications in the determination of biomolecules, such as DNA (Wang et al., 2015), microRNA (Zhang et al., 2015), DNA methylation (Lu et al., 2018), and proteins (Wang et al., 2018b). To increase the sensitivity and adaptability of ECL method, a variety of nucleic acid amplification technologies have been extensively used in the area of biosensors, such as catalyzed-hairpin-assembly amplification (CHA) (Yu et al., 2016; Zhang et al., 2018), hybridization chain reaction (HCR) (Chen et al., 2012), rolling circle amplification (RCA) (Chen et al., 2016), and isothermal strand-displacement polymerase reaction (ISDPR) (Wang et al., 2018a). Among

* Corresponding author.
E-mail address: yanli@nwu.edu.cn (Y. Li).

https://doi.org/10.1016/j.bios.2019.111664
Received 3 June 2019; Received in revised form 10 August 2019; Accepted 28 August 2019
Available online 01 September 2019
0956-5663/

these signal amplification approaches, ISDPR attracted great attention due to its unique merits, such as without the need for specific recognition sites, specially designed circular templates and repeated thermal cycling (Wang et al., 2015, 2018a). In the process of ISDPR, the hybridization between target miRNA and the template can trigger a polymerization reaction with the addition of phi-29 DNA polymerase, which can generate a large quantity of DNA fragments to substitute for the target miRNA (Chen et al., 2015). The released target miRNA hybridizes with the next template to induce a new cycle. After the cycle-after-cycle process of hybridization, polymerization and displacement constantly generate more accurate and specific sequences, leading to amplification of the signal. Thus, in this work, we choose an ISDPR amplification strategy to improve the sensitivity of the miRNA ECL biosensor.

Recently, AuNPs-functionalized DNA biobarcoded nanoprobe emerged as an alternative and facile amplification tool for the development of highly sensitive biosensors due to its well-established conjugation strategies, superior optical and electrical properties (Giljohann et al., 2010; Song et al., 2010). The detection sensitivity can be improved to a certain degree when a large number of thiolated DNA strands are strongly bound to the surfaces of the AuNPs through Au–S bonds (Hu et al., 2008). However, these nucleic acid assays based on AuNPs-biobarcode amplification strategies involve one-to-many recognition reactions between the signal amplification unit and the target DNA. The event of one AuNPs-biobarcode probe hybridized with many target DNAs may lead to low sensitivity for the DNA detection. To further amplify the signal, bridge DNA probes were prepared by the hybridization of ingeniously designed DNA sequences. The bridge DNA could combine with three AuNPs-biobarcodes to form the bridge DNA-AuNPs nanocomposites, which effectively improved the sensitivity and accurately controlled the aggregation of the three AuNPs-biobarcodes (Bo et al., 2018; Zhong et al., 2009). In the designed ECL biosensor, the bridge DNA-AuNPs nanocomposites as carriers for biotin-thiolated DNA probes that were bound much more to the ECL signal probes by the specific interaction between biotin and streptavidin and thus resulting in amplified the ECL signal.

In this work, we fabricated a sensitive and selective ECL biosensor for the detection of microRNA-21 (miRNA-21) as a model target through integrating ISDPR with a bridge DNA-AuNPs nanocomposites dual-signal amplification strategy. The miRNA-21 chosen for this study was of biomedical significance because it participates in the regulation of oncogenic processes and is distinctively overexpressed in a variety of cancer cells (Andorfer et al., 2011). Firstly, this method involved the ISDPR process, which transforms a small number of targets (miRNA-21) into a large number of assistant DNAs. This could be considered the first signal amplification element. Secondly, the bridge DNA-AuNPs nanocomposites were introduced into the detection system, which can bond much more ECL signal probes by the specific interaction between biotin and streptavidin. This is the second signal amplification strategy. Therefore, the designed ECL sensor achieved ultrasensitive detection of the target miRNA-21, which opens a new path for the detection of other biomarkers in biomedical research and therapeutic monitoring. To our knowledge, this is a new example of ECL detection of miRNA based on ISDPR and bridge DNA-AuNPs nanocomposites.

2. Experimental section

2.1. Preparation of streptavidin-modified $Ru(bpy)_3^{2+}$ complex and bridge DNA-AuNPs nanocomposites

A streptavidin-modified Ru $(bpy)_3^{2+}$ complex (SA-Ru) was synthesized according to previous literature (Deiss et al., 2009), which is provided in the supplementary material. The SA-Ru synthesized was characterized by ultraviolet (UV)-vis spectroscopy (Fig. S1). The results indicate that the Ru $(bpy)_3^{2+}$ complex tag was attached to the streptavidin.

AuNPs were synthesized according to previous literature (Ye et al., 2015). The AuNPs synthesized were characterized by transmission electron microscopy (TEM) (Fig. S2A) and dynamic light scattering (DLS) (Fig. S3). The results indicated that the Au nanoparticles were highly monodispersed, with an average diameter of 13 nm. AuNPs-biobarcodes were prepared according to the previous literature with some minor revisions (Bo et al., 2018; Zhang et al., 2006). The glass vials were soaked in chromic acid solution for 1 day and then rinsed with Millipore water before use. In brief, two thiolated probes (DNA probes 1 and 2) were separately dissolved in immobilization buffer (IB) solution [10 mM tris-(hydroxymethyl)aminomethane hydrochloride (Tris–HCl), 1 mM EDTA, 10 mM tris(carboxyethyl)phosphine (TCEP), 0.1 M NaCl, pH 7.4]. Next, 400 μL of 8 μM DNA probe 1 and 200 μL of 8 μM DNA probe 2 were added into 1 mL of AuNPs and shaken gently for 16 h without light. Then, the obtained AuNP-biobarcode nanocomposites were redispersed in 0.1 M phosphate-buffered saline (PBS) with 1.0 M NaCl (pH 7.0) for 24 h (Bo et al., 2018). Afterward, the formed nanocomposites were purified in 10 mM PBS (pH 7.4) containing 0.2 M NaCl through centrifugation (12,000 rpm, 30 min, 4 °C) to remove excess reagents. Finally, the resulting AuNPs-biobarcodes were resuspended in 1 mL of 10 mM PBS containing 0.2 M NaCl (pH 7.4) and stored at 4 °C. The synthesized AuNPs-biobarcodes were characterized by UV–vis spectra (Fig. S2C) (Dong et al., 2015). The results indicate that DNA was successfully modified on the surface of the AuNPs.

The bridge DNA was prepared according to previous literature with minor modifications (Bo et al., 2018; Zhong et al., 2009). In brief, bridge DNA probes 1 and 2 were dissolved separately in TE buffer solution (10 mM Tris-HCl, 1.0 mM EDTA, pH 8.0). Then, 250 μL of 8 μM bridge DNA probe 1 solution and 250 μL of 8 μM bridge DNA probe 2 solution were mixed and heated to 94 °C for 5 min, followed by slowly cooling to room temperature to complete the hybridization reaction. The prepared bridge DNA was kept at 4 °C until use.

The bridge DNA-integrated AuNPs-biobarcode signal amplification unit was prepared as follows (Bo et al., 2018). The synthesized bridge DNA was mixed with the AuNPs-biobarcodes and shaken gently in the dark at 25 °C for 2 h, followed by centrifugation for 30 min at 12,000 rpm to remove excess reagents. Following removal of the supernatant, the red precipitate was rinsed with 10 mM PBS (pH 7.4) containing 0.2 M NaCl and then redispersed in 1 mL of 10 mM PBS (pH 7.4) containing 0.2 M NaCl. The prepared signal amplification unit was stored at 4 °C. The bridge DNA-AuNPs nanocomposites were characterized by TEM (Fig. S2B). The results were consistent with those in a previous report (Jing et al., 2014).

2.2. Isothermal strand-displacement polymerase reaction

The ISDPR was conducted according to previous reports with some minor revision (Zhang et al., 2014; Zeng et al., 2018). The ISDPR was carried out by mixing 20 μL of 1 μM template DNA, 10 μL of 5 X miRNA hybridization buffer, and 20 μL of varying concentrations of target miRNA-21. Then, the mixture was allowed to react at 80 °C for 10 min and slowly cooled to room temperature over approximately 2.5 h to ensure hybridization between the template DNA and miRNA-21. After the addition of a 50 μL solution consisting of 100 U/mL phi29 DNA polymerase, 250 μM dNTPs, 100 U/mL nicking endonuclease (Nt. *Bsm*AI), and 1 × reaction buffer [50 mM Tris-HCL, 10 mM $(NH_4)_2SO_4$, 200 μg/mL BSA, 10 mM $MgCl_2$, 4 mM DTT, 50 mM KCl. pH 7.5], the mixed solution was kept at room temperature for 2.5 h in a constant-temperature incubator to produce assistant DNA. Finally, the reaction was terminated by incubation at 65 °C for 10 min, and the obtained products were stored at 4 °C. The results of Gel electrophoresis suggest that the ISDPR is feasible (Fig. S4).

2.3. Fabrication of the ECL biosensor

A gold disk (Au) electrode (Φ = 2.0 mm) was cleaned according to

our previous method (Ma et al., 2016). Then, 10 μL of the IB (10 mM Tris-HCl, 1 mM EDTA, 10 mM TCEP, 0.1 M NaCl, pH 7.4) containing 0.5 μM thiolated capture probe (SH-CP) was dropped on the cleaned Au electrodes and assembled at room temperature for 12 h. The condition of the SH-CP assembly was based on previous work by our group and other literature (Li et al., 2013; Wei et al., 2017; Cheng et al., 2018). Subsequently, the SH-CP assembled electrode was carefully washed with ultrapure water, and 10 μL of 1 mM 6-mercaptohexanol (MCH) was dropped onto the SH-CP assembled electrode for 1 h to block the nonspecific binding sites. The resulting MCH/SH-CP/-modified Au electrode was then thoroughly washed with hybridization buffer (HB) solution (10 mM Tris-HCl, 1.0 mM EDTA, 1.0 M NaCl, pH 7.4) and used as an ECL biosensing electrode.

2.4. ECL measurements

Before use, the ECL biosensor was incubated with the mixture of the reaction product of the ISDPR at room temperature for 1 h to capture the assistant DNA on the surface of the sensing electrodes by hybridizing with SH-CP. The resulting electrode was labeled as the assistant DNA/MCH/SH-CP/Au electrode. Next, the assistant DNA/MCH/SH-CP/Au electrode was washed two times with HB solution and deionized water and further exposed to the bridge DNA-AuNPs for 1 h (labeled as the bridge DNA-AuNPs/assistant DNA/MCH/SH-CP/Au electrode) and rinsed two times with deionized water to remove nonspecifically adsorbed sequences. Afterward, the SA-Ru was drop-coated onto the electrode surface and allowed to stay for 60 min. The obtained electrode was washed with deionized water and labeled as the SA-Ru/bridge DNA-AuNPs/assistant DNA/MCH/CP/Au electrode. Finally, the resulting electrode was transferred to 1.0 mL of 0.1 M PBS (pH 7.4) containing 50 mM tri-n-propylamine (TPrA) to record the ECL response. The linear potential with a scan rate of 50 mV/s was applied from 0 to 1.2 V (vs. Ag/AgCl) and the ECL signal was recorded.

3. Results and discussion

3.1. Principle of the ECL biosensor

A schematic diagram of the constructed biosensor is provided in Scheme 1. In brief, we first took advantage of the hybridization of two partially complementary sequences (bridge DNA probes 1 and 2) to form bridge DNA. Then, AuNPs-biobarcodes were prepared by two kinds of biotin-thiolated DNA probes and AuNPs via the gold-sulfur affinity. Then, the bridge DNA-AuNPs nanocomposites were formed by mixing the bridge DNA and the AuNPs-biobarcodes. The bridge DNA consisted of a double-stranded middle section and four single-stranded tails; two of the tails were designed to hybridize with DNA probe 1 on the surface of the AuNPs-biobarcodes, the other one could hybridize with DNA probe 2, and the remaining single-stranded tail was used for further hybridization on the surface of the electrode. Thus, the bridge DNA uniquely linked three AuNPs-biobarcodes to achieve a significant sensitivity (as shown in Scheme 1A). In the ISDPR, the target miRNA (miRNA-21 was chosen as a model) could hybridize with the template sequence, and then the microRNA-21 can be extended from its 3′ terminal to the 5′ terminal of the template DNA to form a double stranded DNA in the presence of dNTPs and phi29 DNA polymerase. Meanwhile, a recognition site for the Nt. *Bsm*AI was generated, which initiated Nt. *Bsm*AI to cut one strand nick of DNA on a double-stranded DNA. The subsequent strand displacement synthesis extended the 3′-end at the nick, and the downstream DNA strand (labeled assistant DNA) could be displaced and released. The release of the assistant DNA could lead to another round of polymerase reaction of the miRNA-21 and the generation of plenty of assistant DNA. As a result, the target miRNA was cyclically reused and assistant DNA was released, resulting in signal amplification of the target (as shown in Scheme 1B). Therefore, we conclude that the ISDPR can be regarded as the second signal amplification element. After the completion of the ISDPR, the assistant DNA was captured by the SH-CP self-assembled on the Au electrode and further hybridized with the fourth single-stranded end of the bridge DNA to immobilize the bridge DNA-AuNPs nanocomposites. As a consequence of the bridge DNA linking three AuNPs-biobarcodes, a large quantity of biotin groups was introduced into the sensing platform. Thus, more ECL signal probe SA-Ru could be linked to the surface of the bridge DNA-AuNPs nanocomposites by the specific interaction between biotin and streptavidin, leading to a significant enhancement of the ECL intensity (as shown in Scheme 1C). This ECL signal response was proportional to the amount of SA-Ru within a certain range, which in turn indicated the concentration of target miRNA-21. The processes of preparing the signal-on ECL biosensor were characterized by cyclic voltammograms (CVs) and electrochemical impedance spectra (EIS). The results (Fig. S5A, Fig. S5B) demonstrated that the biosensor was successfully fabricated and bound with assistant DNA and bridge DNA-AuNPs nanocomposites.

3.2. Investigation of the bridge DNA-AuNPs nanocomposites

We investigated the amplification efficiency of the bridge DNA-AuNPs nanocomposites. Fig. 1 presents the ECL intensity of the biosensor under different conditions. A much lower ECL response was observed in the SH-CP self-assembled on the electrode (curve a), which was ascribed to the fact that the ECL probe SA-Ru was not captured on the electrode. In contrast, the ECL signal was increased to some extent in the presence of the DNA probe 3-modified AuNPs-biobarcodes (curve b). DNA probe 3 was designed with the complementary sequence to the assistant DNA. As a result, the DNA probe 3-modified AuNPs-biobarcodes could be employed to hybridize with the assistant DNA so that the ECL species SA-Ru could be fixed on the surfaces of the AuNPs-biobarcodes. The ECL intensity was significantly amplified when the bridge DNA-AuNPs nanocomposites were captured by assistant DNA sequences (curve c). The reason for this observation is that the bridge DNA linked three AuNPs-biobarcodes, leading to ECL probe SA-Ru composites being bound to the surface of the biosensor. The results suggested that the bridge DNA-AuNPs nanocomposites could significantly improve the performance of the ECL biosensor.

3.3. Feasibility study

The feasibility of this protocol was investigated by comparing the ECL signal of electrodes with and without the signal amplification unit. From Fig. 2, it can be seen that a weak ECL signal can be detected by the MCH/SH-CP/Au electrode, due to there is no target miRNA (curve a). The ECL intensity from the sample without target miRNA with amplification (curve c) was just a little higher than that from the MCH/SH-CP/Au electrode (curve a) whose ECL response could be ascribed to the nonspecific adsorption of SA-Ru on the electrode surface. With addition of the target miRNA, the other control experiments, those without bridge DNA-AuNPs nanocomposites (curves b) or without ISDPR (curve d), were performed. The results showed only small or weakly increased MCH/SH-CP/Au electrode ECL signals, which could be attributed to the fact that the ECL signal probe SA-Ru could not be effectively linked to the surface of the biosensing electrode by the specific interaction. In the presence of miRNA-21 (10 fM), the ISDPR proceeded to produce abundant assistant DNA that could be used to hybridize with the SH-CP on the biosensing electrode. The introduction of the assistant DNA led to an evident increase in the ECL response (curve e), suggesting that the bridge DNA-AuNPs nanocomposites had been successfully hybridized with the assistant DNA and that the ECL signal probe SA-Ru was linked to the surface of the biosensing electrode by the specific interaction between biotin and streptavidin. When the concentration of miRNA-21 was increased from 10 fM to 10,000 fM, the ECL response was further increased (curve f), indicating that the ECL response was closely associated with the miRNA-21 concentration. The experimental results

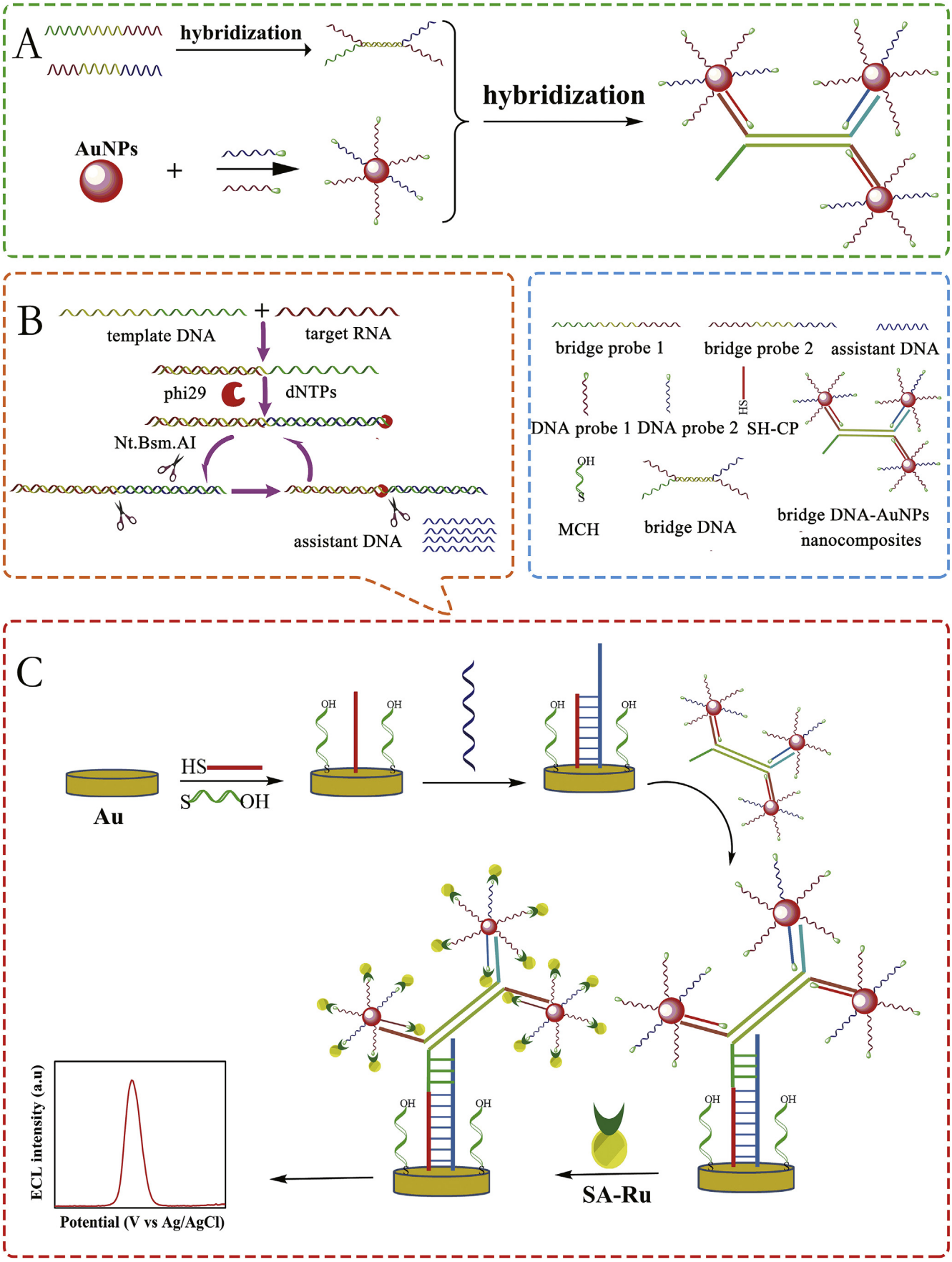

Scheme 1. Schematic diagram of the proposed ECL-based biosensor for miRNA-21 detection: (A) The preparation process of the bridge DNA-AuNPs nanocomposites. (B) The target-induced cycling reaction based on the phi29-mediated ISDPR. (C) The ECL biosensor for miRNA analysis based on bridge DNA-AuNPs nanocomposites and the ISDPR.

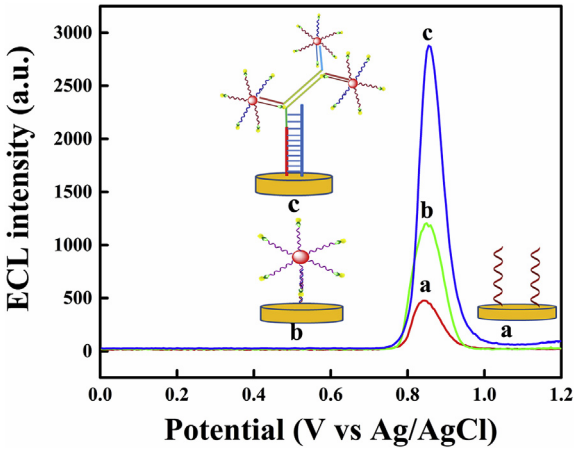

Fig. 1. ECL intensity vs potential profiles of the biosensors for (a) the self-assembled SH-CP–modified Au electrode, (b) capture of DNA probe 3-modified AuNPs-biobarcodes after the completion of the ISDPR in the presence of miRNA-21, and (c) after capture of the bridge DNA-AuNPs nanocomposites. The ECL signals were measured in 0.1 M PBS containing 50 mM TPrA (pH 7.4) by scanning the potential from 0 to 1.2 V (vs. Ag/AgCl) at a scanning rate of 50 mV/s.

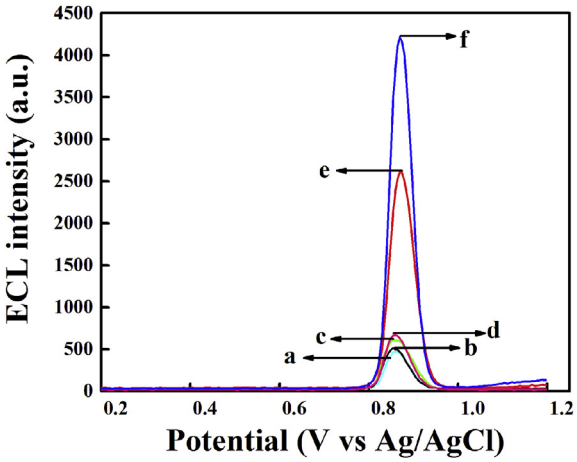

Fig. 2. ECL responses of the sensing electrodes for (a) the absence of miRNA-21 without ISDPR and bridge DNA-AuNPs nanocomposites, (b) the presence of miRNA-21 (10 fM) with ISDPR but without bridge DNA-AuNPs nanocomposites, (c) the absence of miRNA-21 (10 fM) with ISDPR and bridge DNA-AuNPs nanocomposites, (d) the presence of miRNA-21 (10 fM) without ISDPR with bridge DNA-AuNPs nanocomposites, (e) the presence of miRNA-21 (10 fM), and (f) miRNA-21 (10,000 fM) with ISDPR and bridge DNA-AuNPs nanocomposites. The immobilization concentration of SH-CP was 0.5 μM, the concentration of template DNA was 1 μM, the ISDPR incubation time was 60 min, and the bridge DNA-AuNPs hybridization time was 60 min.

clearly indicated the apparent signal amplification ability of the established strategy via the integration of the ISDPR and bridge DNA-AuNPs nanocomposites dual-signal amplification strategy. Therefore, the developed dual-signal amplification means was feasible for the further detection of miRNA-21.

3.4. Performance of the ECL biosensor for miRNA-21

Under optimal conditions (Fig. S6), different concentrations of miRNA-21 were detected by the ECL biosensor. Fig. 3A shows the ECL responses versus potential profiles from the biosensor with different concentration of miRNA-21. The ECL intensity is logarithmically proportion to the concentration of the miRNA-21 in the range 0.01 fM to 10,000 fM. The regression equation was $I = 493.92 \log c + 9258.74$ (where I and c refer to the ECL intensity and miRNA-21 concentration, respectively), and the square of the correlation coefficient (R) was 0.9992, with a detection limit estimated to be 3.2 aM (Fig. 3B). As shown in Table 1, the linear range of the developed method is much wider than that of previously reported miRNA-21 assays. The detection limit of the signal-on ECL biosensor with the dual-signal amplification strategy in this work was a few orders of magnitude lower than those of previous methods for miRNA-21 detection except Wen et al.'s work (Wen et al., 2012). The detection limit of the signal-on ECL biosensor for miRNA-21 in this work (3.2 aM) was slight lower than that (6.8 aM) using the analogous electronic biosensing scheme reported by Bo et al. (2018). As described above, the low detection limit in this work can be explained by the ISDPR process, which transformed a small number of targets (miRNA-21) into a large number of assistant DNAs and bridge DNA-AuNPs nanocomposites as carriers for biotin-thiolated DNA probes which bound much more ECL signal probes by the specific interaction between biotin and streptavidin.

To explore the selectivity of the ECL method, miRNA-199a, miRNA-141, and miRNA-155 were selected as interfering agents. As shown in Fig. 3C/D, the ECL signals of miRNA-199a, miRNA-141, and miRNA-155 did not exhibit any substantial increase compared with that of the blank sample. By contrast, when the mixture solution (1000 fM miRNA-21 containing 10 pM miRNA-199a, 10 pM miRNA-141, and 10 pM miRNA-155) was investigated, the ECL intensity of the biosensor presented an ECL intensity similar to that observed after incubating the biosensor with the miRNA-21 (1000 fM), which indicated that the interference factors had negligible influence on the response to miRNA-21. The results indicate that the ECL method developed in this work had good selectivity.

Reproducibility is another important factor when evaluating a method for practical application. To monitor the reproducibility of the biosensor, seven identical biosensors were constructed with miRNA-21 concentrations of 10 fM. As shown in Fig. 3E, the seven biosensors exhibited similar ECL responses, with a relative standard deviation (RSD) of 2.21%. This result indicates that the fabricated detection strategy has acceptable reproducibility.

3.5. Detection of miRNA-21 in cancer cells

To further verify the applicability and feasibility of the method, human breast cancer cells (MCF-7) were chosen for ECL assays to monitor the expression of miRNA-21 biomarkers in cancer cells. The cell samples were treated with a commercial miRNA extraction kit after cell counting. Then, the sensitivity was investigated with cell numbers from 10 cells to 10^4 cells. As observed from Fig. 4, when the number of MCF-7 cells increased from 10 cells to 10^4 cells, the ECL signal increased gradually. From the results in Fig. 4 and the aforementioned linear regression equation, we determined that the miRNA-21 concentrations of the MCF-7 cell lysates 10 cells, 100 cells, 1000 cells, 5000 cells, and 10,000 cells were 0.02 fM, 0.032 fM, 0.1 fM, 1 fM and 22 fM, respectively. The amount of miRNA-21 detected in MCF-7 cells (the normal expression of miRNA-21) was approximately 2408 molecules per cell, which is in good accordance with other literature (Yang et al., 2014; Zhang et al., 2013). The reliability of the proposed method was also tested by recovery experiments, which were performed via spiking miRNA-21 with different concentrations into MCF-7 total miRNA extract samples. The obtained results (Table S2 in the Supporting Information) show the acceptable relative standard deviation and quantitative recoveries, indicating that the present ECL biosensor could be applied to the sensitive detection of miRNA-21 in real samples.

4. Conclusions

In summary, a signal-on ECL biosensor for the detection of miRNA-21 was constructed based on a dual-signaling amplification strategy (ISDPR and bridge DNA-AuNPs nanocomposites). The assay exhibited

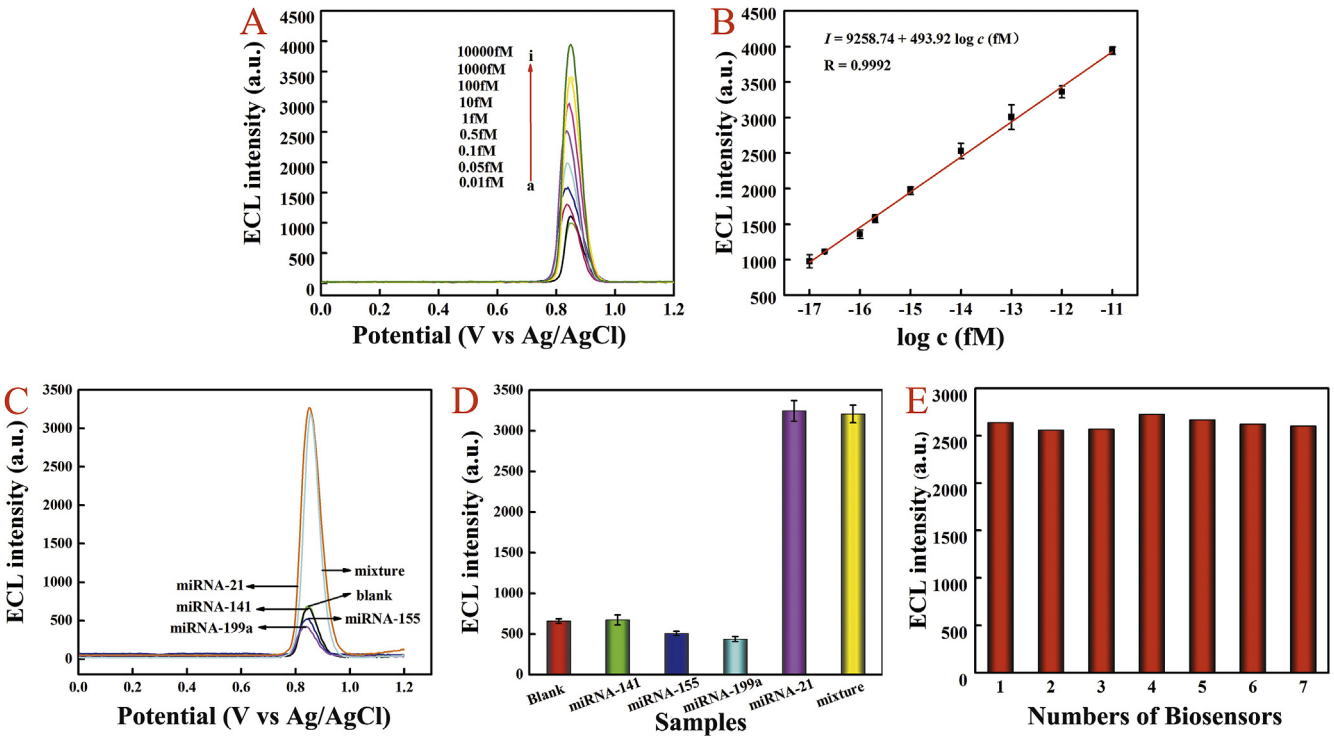

Fig. 3. (A) ECL responses to different concentrations of miRNA-21 (from a to i, 0.01 fM, 0.05 fM, 0.1 fM, 0.5 fM, 1 fM, 10 fM, 100 fM, 1000 fM, 10,000 fM, respectively). (B) The linear relationship between ECL intensity and the logarithm miRNA-21 concentrations. Error bars are standard deviations obtained from three independent experiments. (C, D) The ECL responses of the biosensor to different interfering nucleic acids: blank, miRNA-141 (10 pM), miRNA-155 (10 pM), miRNA-199a (10 pM), and a mixture of these nucleic acids (containing 1 pM miRNA-21, 10 pM miRNA-141, 10 pM miRNA-155, 10 pM miRNA-199a). (E) The reproducibility of seven biosensors fabricated identically toward miRNA-21 of 10 fM.

Table 1
Comparison of different methods for miRNA-21 detection.

Methods	Linear range (M)	LOD (M)	Reference
Electrochemistry	10^{-16} - 1.5 × 10^{-12}	3.3 × 10^{-17}	Gai et al. (2017)
Electrochemistry	10^{-15} - 10^{-10}	6.4 × 10^{-16}	Yang et al. (2015)
Electrochemistry	10^{-14} - 5.0 × 10^{-12}	3.0 × 10^{-15}	Liu et al. (2014a)
Electrochemistry	2.0 × 10^{-12} - 2.0 × 10^{-7}	2.0 × 10^{-12}	(Poehlmann et al., 2010)
Electrochemistry	5.0 × 10^{-15}- 5.0 × 10^{-11}	3.0 × 10^{-15}	Yang et al. (2014)
Electrochemistry	10^{-17}- 10^{-11}	6.8 × 10^{-18}	Bo et al. (2018)
Fluorescence	10^{-12} - 10^{-8}	1.0 × 10^{-13}	Zhang et al. (2013)
Fluorescence	10^{-14} - 10^{-11}	7.3 × 10^{-15}	Lv et al. (2016)
Fluorescence	10^{-10} - 8.0 × 10^{-6}	6.0 × 10^{-11}	Lu et al. (2017)
Colorimetry	10^{-17} - 10^{-12}	2.0 × 10^{-18}	Wen et al. (2012)
Photoelectrochemical	5 × 10^{-15} - 2.5 × 10^{-12}	1.67 × 10^{-15}	Wang et al. (2014)
Chemiluminescence	5 × 10^{-15} - 5 × 10^{-11}	1.7 × 10^{-15}	Chen et al. (2019)
SERS	10^{-14} - 10^{-8}	2.33 × 10^{-15}	Wang et al. (2019)
SERS	10^{-15} - 10^{-8}	6.7 × 10^{-16}	Yang et al. (2018b)
ECL	10^{-16} - 10^{-9}	1.07 × 10^{-17}	Jiang et al. (2019)
ECL	10^{-16} - 10^{-10}	3.6 × 10^{-17}	Zhou et al. (2018)
ECL	10^{-15} - 10^{-9}	5 × 10^{-16}	Feng et al. (2016)
ECL	10^{-17} - 10^{-11}	3.2 × 10^{-18}	This work

excellent specificity and ultrahigh sensitivity with a detection limit of 3.2 aM, and it had an extremely large dynamic range of six orders of magnitude in the range from 0.01 fM to 10,000 fM. Furthermore, the proposed strategy successfully detected miRNA-21 in total RNA samples extracted from human breast cancer cells. However, ISDPR amplification element in this work suffered from negative factors, involving high cost and potential instability due to enzyme-dependent. The negative factors can be resolved if enzyme-free amplification based on oligonucleotide strategy was used to fabricate an ECL biosensor. Further works on these projects are in progress going to the ECL detection of other cancer-related nucleic acids.

CRediT authorship contribution statement

Aiping Cui: Conceptualization, Data curation, Formal analysis, Investigation, Methodology, Writing - original draft, Writing - review & editing. **Jianwei Zhang:** Validation, Writing - review & editing. **Wanqiao Bai:** Conceptualization, Software. **Huiping Sun:** Writing - original draft. **Lin Bao:** Investigation, Project administration. **Fen Ma:** Investigation. **Yan Li:** Funding acquisition, Resources, Writing - review & editing.

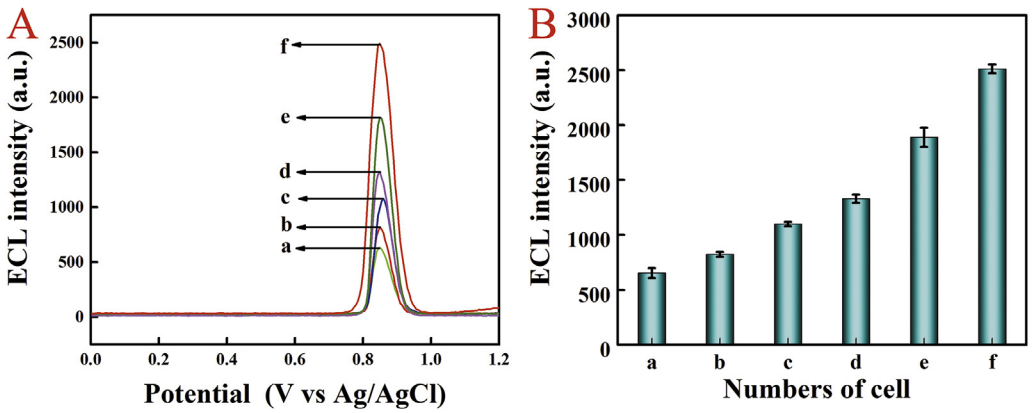

Fig. 4. (A, B) Application of the biosensor in tumor cell line detection: (a) blank, (b) 10 cells, (c) 10^2 cells, (d) 10^3 cells, (e) 5×10^3 cells, and (f) 10^4 cells of the human breast cancer (MCF-7) cell line. The measurement conditions were the same as those described in Fig. 1.

Declaration of competing interest

The authors declare that they have no known competing financial interests or personal relationships that could have appeared to influence the work reported in this paper.

Acknowledgements

This work was supported by the National Natural Science Foundation of China (Nos. 21675124 and 21375102) and Key Laboratory of Yulin Desert Plant Resources.

Appendix A. Supplementary data

Supplementary data to this article can be found online at https://doi.org/10.1016/j.bios.2019.111664.

References

Andorfer, C.A., Necela, B.M., Thompson, E.A., Perez, E.A., 2011. Trends Mol. Med. 17, 313–319.
Bo, B., Zhang, T., Jiang, Y., Cui, H., Miao, P., 2018. Anal. Chem. 90, 2395–2400.
Chen, C., Ridzon, D.A., Bromer, A.J., Zhou, Z., Lee, D.H., Nquyen, J.T., Barbisin, M., Xu, N.L., Mahuvakar, V.R., Andersen, M.R., Lao, K.Q., Livak, K.J., 2005. Nucleic Acids Res. 27, e179.
Chen, Y., Xu, J., Su, J., Xiang, Y., Yuan, R., Chai, Y., 2012. Anal. Chem. 84, 7750–7755.
Chen, A., Gui, G., Zhuo, Y., Chai, Y., Xiang, Y., Yuan, R., 2015. Anal. Chem. 87, 6328–6334.
Chen, A., Ma, S., Zhuo, Y., Chai, Y., Yuan, R., 2016. Anal. Chem. 88, 3203–3210.
Chen, D., Wen, S., Peng, R., Gong, Q., Fei, J., Fu, Z., Weng, C., Liu, M., 2019. Microchim. Acta. 186, 410.
Cheng, H., Liu, J., Ma, W.J., Duan, S.D., Huang, J., He, X.X., Wang, K.M., 2018. Anal. Chem. 90, 12544–12552.
Deiss, F., LaFratta, C.N., Symer, M., Blicharz, T.M., Sojic, N., 2009. J. Am. Chem. Soc. 131, 6088–6089.
Deng, R., Zhang, K., Li, J., 2017. Acc. Chem. Res. 50 (4), 1059–1068.
Dong, H., Meng, X., Dai, W., Cao, Y., Lu, H., Zhou, S., 2015. Anal. Chem. 87, 4334–4340.
Feng, Q.M., Shen, Y.Z., Li, M.X., Zhang, Z.L., Zhao, W., Xu, J.J., Chen, H.Y., 2016. Anal. Chem. 88, 937–944.
Gai, P., Gu, C., Li, H., Sun, X., Li, F., 2017. Anal. Chem. 89, 12293–12298.
Giljohann, D.A., Seferos, D.S., Daniel, W.L., Massich, M.D., Patel, P.C., Mirkin, C.A., 2010. Angew. Chem. Int. Ed. 49, 3280–3294.
Git, A., Dvinge, H., Salmon-Divon, M., Osborne, M., Kutter, C., Hadfield, J., Bertone, P., Caldas, C., 2010. RNA 16, 1–16.
Hansen, T.B., Jensen, T.I., Clausen, B.H., Bramsen, J.B., Finsen, B., Damgaard, C.K., Kjems, J., 2013. Nature 495, 384–388.
Hu, K., Lan, D., Li, X., Zhang, S., 2008. Anal. Chem. 80, 9124–9130.
Jiang, X., Wang, H., Chai, Y., Li, H., Shi, W., Yuan, R., 2019. Anal. Chem. 91, 10258–10265.
Jing, X., Cao, X., Wang, L., Lan, T., Li, Y., Xie, G., 2014. Biosens. Bioelectron 58, 40–47.
Lee, R.C., Ambros, V., 2001. Science 294, 862–864.
Li, Y., Huang, C.C., Zheng, J.B., Qi, H.L., 2013. Talanta 103, 8–13.
Li, Y., Wen, S., Yao, X., Liu, W., Shen, J., Deng, W., Tang, J., Li, C., Liu, K., 2017. Cell Death Dis. 8, e3127.
Liang, R.Q., Li, W., Li, Y., Tan, C.Y., Li, J.X., Jin, Y.X., Ruan, K.C., 2005. Nucleic Acids Res. 33, e17.
Liu, L., Xia, N., Liu, H., Kang, X., Liu, X., Xue, C., He, X., 2014a. Biosens. Bioelectron. 53, 399–405.
Liu, Y., Lei, J., Huang, Y., Ju, H., 2014b. Anal. Chem. 86, 8735–8741.
Liu, Z., Qi, W., Xu, G., 2015. Chem. Soc. Rev. 44, 3117–3142.
Lu, S., Wang, S., Zhao, J., Sun, J., Yang, X., 2017. Anal. Chem. 89, 8429–8436.
Lu, L., Wang, J., Miao, W., Wang, X., Guo, G., 2018. Anal. Chem. 91, 1452–1459.
Lv, W., Zhao, J., Situ, B., Li, B., Ma, W., Liu, J., Wu, Z., Wang, W., Yan, X., Zheng, L., 2016. Biosens. Bioelectron. 83, 250–255.
Ma, S., Sun, H., Li, Y., Qi, H., Zheng, J., 2016. Anal. Chem. 88, 9934–9940.
Poehlmann, C., Sprinzl, M., 2010. Anal. Chem. 82, 4434–4440.
Song, S., Qin, Y., He, Y., Huang, Q., Fan, C., Chen, H.Y., 2010. Chem. Soc. Rev. 39, 4234–4243.
Tian, L., Qi, J., Ma, X., Wang, X., Yao, C., Song, W., Wang, Y., 2018. Biosens. Bioelectron. 122, 43–50.
Wang, M., Yin, H.S., Shen, N.N., Xu, Z.N., Sun, B., Ai, S.Y., 2014. Biosens. Bioelectron. 53, 232–237.
Wang, X., Ge, L., Yu, Y., Dong, S., Li, F., 2015. Sens. Actuators, B 220, 942–948.
Wang, M., Zhou, Y., Yin, H., Jiang, W., Wang, H., Ai, S., 2018a. Biosens. Bioelectron. 107, 34–39.
Wang, X., Gao, H., Qi, H., Gao, Q., Zhang, C., 2018b. Anal. Chem. 90, 3013–3018.
Wang, Z.X., Ye, S.J., Zhang, N., Liu, X., Wang, M.L., 2019. Anal. Chem. 91, 5043–5050.
Wei, Y.Y., Sun, H.P., Li, J., Zhang, Y.L., Li, Y., Lin, J.X., Wang, T.S., Zhou, M., 2017. J. Electroanal. Chem. 795, 123–129.
Wen, Y., Xu, Y., Mao, X.H., Wei, Y., Song, H., Chen, N., Huang, Q., Fan, C., Li, D., 2012. Anal. Chem. 84, 7664–7669.
Yang, C., Dou, B., Shi, K., Chai, Y., Xiang, Y., Yuan, R., 2014. Anal. Chem. 86, 11913–11918.
Yang, C., Shi, K., Dou, B., Xiang, Y., Chai, Y., Yuan, R., 2015. ACS Appl. Mater. Interfaces 7, 1188–1193.
Yang, Q., Gu, W.W., Gu, Y., Yan, N.N., Mao, Y.Y., Zhen, X.X., Wang, J.M., Yang, J., Shi, H.J., Zhang, X., Wang, J., 2018a. J. Transl. Med. 16, 186.
Yang, X., Wang, S., Wang, Y., He, Y., Chai, Y., Yuan, R., 2018b. ACS Appl. Mater. Interfaces 10, 12491–12496.
Ye, S., Wu, Y., Zhai, X., Tang, B., 2015. Anal. Chem. 87, 8242–8249.
Yu, Y.Q., Wang, J.P., Zhao, M., Hong, L.R., Chai, Y.Q., Yuan, R., Zhuo, Y., 2016. Biosens. Bioelectron. 77, 442–450.
Yuen, T., Wurmbach, E., Pfeffer, R.L., Ebersole, SealfonS., 2002. Nucleic Acids Res. 30, e48.
Zeng, R., Su, L., Luo, Z., Zhang, L., Lu, M., Tang, D., 2018. Anal. Chim. Acta 1038, 21–28.
Zhang, J., Song, S., Zhang, L., Wang, L., Wu, H., Pan, D., Fan, C., 2006. J. Am. Chem. Soc. 128, 8575–8580.
Zhang, M., Liu, Y.L., Yu, C.Y., Yin, B.C., Ye, B.C., 2013. Analyst 138, 4812–4817.
Zhang, Q., Chen, F., Xu, F., Zhao, Y., Fan, C., 2014. Anal. Chem. 86, 8098–8105.
Zhang, P., Wu, X., Yuan, R., Chai, Y., 2015. Anal. Chem. 87, 3202–3207.
Zhang, Y., Li, Z., Chai, Y., Wang, H., Yuan, R., 2018. Chem. Commun. 54, 10148–10151.
Zhong, H., Lei, X., Hun, X., Zhang, S., 2009. Chem. Commun. 45, 6958–6960.
Zhou, Y., Wang, H., Zhang, H., Chai, Y., Yuan, R., 2018. Anal. Chem. 90, 3543–3549.